Physical Mechanisms for Chemotactic Pattern Formation by Bacteria

Michael P. Brenner,* Leonid S. Levitov,# and Elena O. Budrene§

Departments of *Mathematics and #Physics, Massachusetts Institute of Technology, Cambridge, Massachusetts 02139, and §Department of Cellular and Molecular Biology, Harvard University, Cambridge, Massachusetts 02138 USA

ABSTRACT   This paper formulates a theory for chemotactic pattern formation by the bacteria *Escherichia coli* in the presence of excreted attractant. In a chemotactically neutral background, through chemoattractant signaling, the bacteria organize into swarm rings and aggregates. The analysis invokes only those physical processes that are both justifiable by known biochemistry and necessary and sufficient for swarm ring migration and aggregate formation. Swarm rings migrate in the absence of an external chemoattractant gradient. The ring motion is caused by the depletion of a substrate that is necessary to produce attractant. Several scaling laws are proposed and are demonstrated to be consistent with experimental data. Aggregate formation corresponds to finite time singularities in which the bacterial density diverges at a point. Instabilities of swarm rings leading to aggregate formation occur via a mechanism similar to aggregate formation itself: when the mass density of the swarm ring exceeds a threshold, the ring collapses cylindrically and then destabilizes into aggregates. This sequence of events is demonstrated both in the theoretical model and in the experiments.

INTRODUCTION

Over the last 25 years, there has been a rapidly growing understanding of the mechanisms through which *Escherichia coli* moves in response to external conditions (Berg, 1988). By focusing on how a single bacterium responds to its environment, a microscopic picture of how bacteria process external information has emerged.

Under normal conditions, an *E. coli* cell consists of an elongated body, to which several flagella are attached. Each flagellum is propelled by a rotary motor. There are two modes of operation of this motor, clockwise and counterclockwise. When the individual flagella rotate counterclockwise, they form a bundle, and this bundle propels the bacterium forward (Block and Berg, 1984; Blair and Berg, 1988); when the flagellum turns clockwise, the motions of the individual flagella are independent of each other, causing the cell to randomly change its orientation. These two types of behavior were discovered by Berg and Brown (1972), who dubbed the forward propulsion stage (counterclockwise rotation) "runs" and the erratic turning stage (clockwise rotation) "tumbles." The motion of the cell over long times is determined by the distribution of runs and tumbles. The mean of a run is on the order of $\tau \approx 1$ s, whereas the mean time for tumbles is an order of magnitude shorter. If v is the propulsion speed during the run, the *E. coli* cells perform a random walk with diffusion constant $D = v^2\tau$.

The environment must contain chemicals so that the bacterium can live and function normally. Bacteria require a carbon source, an energy source, and inorganic salts.

Typical assays for motility are engineered so that there are sufficient nutrients for normal survival; if, however, these nutrients are used up, there can be transitions in the internal state of the bacteria, affecting their motion. For example, when bacteria exhaust the exogenous carbon source, their motility increases transiently (Amsler et al., 1993). On the other hand, exhausting oxygen causes the bacteria to immediately stop moving (Khan and Macnab, 1980). Another common environmental response is chemotaxis (Pfeffer, 1884; Stock and Surette, 1996), in which cells move up an external chemical gradient. This response has an origin different from that of the physiological response described above: chemotaxis does not occur to fulfill an immediate nutritional need, nor does it necessarily reflect an attempt to avoid starvation. Indeed, cells can undergo chemotaxis toward attractants that do not serve any metabolic process whatsoever.

For *E. coli*, chemotaxis occurs by constant sampling of attractant as they move. Careful measurements demonstrate that the bacteria compute a weighted difference between the amount of attractant that binds to their receptors during the previous second of motion and the amount of attractant that has bound during the three preceding seconds (Segall et al., 1986). The weighting function used for this computation was directly measured in impulse response experiments on single bacteria. When the convolution of the weighting function with a stimulus is positive, the probability of tumbling decreases; this effectively increases the length of runs in directions of increasing attractant gradient.

The combined effect of the physiological and chemotactic responses of the bacteria motion results in nontrivial collective behaviors, which have been the focus of inquiry since Adler's introduction of assays in which *E. coli* move in migrating "bands." In Adler's experiments, the bands form when cells of *E. coli* are placed in an environment containing substances (oxygen, amino acids, etc.) that the bacteria both consume and respond to chemotactically. The

consumption of the substance generates an attractant gradient, which provokes chemotaxis. The net response is a well-defined band of cells moving across a capillary tube or a petri dish (Adler, 1966, 1969).

Recently, Budrene and Berg (1991, 1995) found conditions in which more complex patterns can form in an environment that is chemotactically inert. In contrast to Adler's experiments, the environmental conditions induce the bacteria to excrete an attractant (aspartate) toward which they undergo chemotaxis. The excretion of attractant means that there is effectively a long-range interaction among the bacteria. These conditions produce patterns that are dramatically different from Adler's initial experiments. Typical experiments are performed on agar plates, in which the agar concentration is low enough that the bacteria can move freely. The type of pattern depends strongly on the amount of a single carbon and energy source (succinate) that is uniformly distributed in the dish. Exposure to succinate is required for bacteria to perform intracellular reactions producing the attractant. At low succinate concentrations, the bacteria originate in the center of the petri dish and form a swarm ring that propagates toward the boundary. At higher succinate concentrations the swarm ring destabilizes and produces a symmetrical array of dense compact structures called aggregates.

The focus of the present paper is to present a theoretical framework for understanding these experimental results. An adequate theory requires understanding which aspects of the phenomenology are chemotactic, and which aspects reflect the changing chemical environment around the *E. coli*. Our analysis will show that the movement of the swarm rings is due to the depletion of succinate around the band of bacteria: chemotaxis holds the band together, but the net motion is not caused directly by chemotactic fluxes. In contrast, aggregates result from a purely chemotactic response in the system, depending only weakly on environmental conditions. As long as the bacteria produce attractant, it is possible for aggregates to form.

MATHEMATICAL MODEL

There is a long history of mathematical modeling of bacterial pattern formation. The basic equations for the bacterial density ρ and the attractant field c are

$$\partial_t \rho = D_b \nabla^2 \rho - \nabla \cdot (k\rho \nabla c) + a\rho \qquad (1)$$

$$\partial_t c = D_c \nabla^2 c + \alpha \rho. \qquad (2)$$

Equations of this type were first introduced (in this context) by Keller and Segal (1970), and (with variations) have been the subject of extensive investigations (see, e.g., Murray, 1989; Oster and Murray, 1989). Here D_b is the bacterial diffusion constant, k is the chemotactic coefficient, a is the rate of bacteria division, α is the rate of attractant production or consumption, and D_c is the chemical diffusion constant. Equation 1 includes the diffusion of bacteria, a chemotactic drift, and division of bacteria. Equation 2 expresses the diffusion and production of attractant.

For *E. coli*, Schnitzer et al. established a direct connection (Schnitzer et al., 1990; Schnitzer, 1993) between the parameters governing the dynamics of the bacterial density (D_b and k) and time-averaged properties of the impulse response function. There is, therefore, a direct connection between the response function of a single bacterium and the collective response of macroscopically many bacteria, providing a rigorous justification for the equations for the density ρ and c.

However, several recent numerical studies (Bruno, 1992; Woodward et al., 1995; Ben-Jacob et al., 1995; Tsimring et al., 1995; Tyson, 1996; Tyson et al., unpublished manuscript) have argued that the physical processes included in Eqs. 1 and 2 are insufficient to explain the Budrene-Berg experiments. In these works several qualitatively different physical mechanisms were proposed for modeling (numerically generated) patterns that roughly "look like" the experiments. The invoked mechanisms ranged from simple variations on the model such as nonlinearity in the chemotactic coefficient (Woodward et al., 1995; Keller and Segel, 1970), to novel ideas such as the existence of a second repellent field or the autocatalytic production of attractant triggered by waste (Ben-Jacob et al., 1995; Tsimring et al., 1995). Because all of these studies produced pictures that look qualitatively like the experiments, it is unclear which specific features are responsible for the pattern formation.

The goal of this paper is to formulate a minimal theory to explain the most robust features of the existing experiments, using known information about the physiological responses of the individual *E. coli*. We seek the most simplified model that is consistent with the known biochemistry and reproduces the key phenomonological aspects of the experiments. It will turn out that, as anticipated by the experiments (Budrene and Berg, 1995), all that is necessary for the pattern formation is the bacterial density, the attractant, and a chemical that is necessary for the production of attractant by the bacteria. (Recent work (Tyson, 1996; Tyson et al., unpublished manuscript) has also simulated a model with only these three ingredients, in an effort to reproduce the large-scale patterns of the Budrene-Berg experiments. The present work focuses more closely on the mechanisms for ring propagation and aggregate formation.) The model leads to analytic solutions corresponding to both rings and aggregates. The analysis yields qualitative predictions and scaling laws relating observable quantities. These predictions are in good agreement with existing experiments.

Below we discuss separately the two main structures that are observed in the Budrene-Berg experiments, rings and aggregates. Ring motion occurs on a slow, metabolic time scale, dictated by the details of the processes through which the bacteria convert chemicals in their environment into attractant. In contrast, the instability of the rings and the formation of aggregates are largely independent of the details of the environmental conditions, and depend only on

coarse properties, such as chemotaxis and production of attractant by bacteria.

RING DYNAMICS

In this section we formulate a theory for the dynamics of swarm rings. Because the motion of the rings is slow, metabolic effects are important, and it is necessary to determine which environmental conditions cause the ring to move. It will turn out that contrary to what might be expected from dynamical Eqs. 1 and 2, the relevant nonlinearities causing propagating rings is not the chemotactic flux term, but instead involves the rate of attractant production.

It is useful to begin by listing the time scales of the competing physical processes operating during swarm ring migration: consider a ring with characteristic thickness L and traveling velocity U. The time that it takes for the ring to move over its thickness is $\tau_C = L/U$. The time needed for the attractant to diffuse over the ring is $\tau_D = L^2/D_c$. For the Budrene-Berg experiments, $L \approx 10^{-1}$ cm, and $U \approx 1/3 \times 10^{-4}$ cm/s, yielding $\tau_C = 3 \times 10^3$/s, $D_c = 10^{-5}$ cm^2/s and $\tau_D \approx 10^3$ s. The other important characteristic time scale is that of bacterial division: the doubling time is around $\tau_{\text{div}} = 10^4$ s. These estimates give the ordering $\tau_D < \tau_C < \tau_{\text{div}}$. The fastest process in the vicinity of the ring is the diffusion of attractant, and the slowest process is cell division.

This separation of time scales suggests two approximations for the local solution in the neighborhood of a ring. First, cell division only weakly modifies the structure around the swarm ring, and so can be neglected. (Cell division does induce a slow time variation of the number of bacteria in the ring. This has important consequences for the dynamics, and will be considered in a subsequent section.) Second, in the vicinity of the ring the attractant diffuses much faster than the ring moves. Under these assumptions, Eqs. 1 and 2 become

$$\partial_t \rho = \nabla^2 \rho - \nabla \cdot (\rho \nabla c) \qquad (3)$$

$$0 = \nabla^2 c + \rho, \qquad (4)$$

where we have nondimensionalized by choosing the density scale $D_c D_b/(\alpha k L^2)$, the attractant scale D_b/k, and the characteristic time scale L^2/D_b.

These equations are incapable of reproducing the ring solutions seen in the experiments. To see this, we use the transformation $v = \nabla c$ and $\rho = -\nabla \cdot v$, yielding the equation for v:

$$\partial_t v + (\nabla \cdot v)v = \nabla \nabla \cdot v \qquad (5)$$

In one dimension, this is the well-known Burgers equation (Burgers, 1948). This relationship between the chemotactic equations and Burger's equations was noted independently by R. E. Goldstein (private communication). A solution of Eq. 5 for a traveling ring with mass per unit length M_0 is given by $v = M_0 \tanh(M_0(x - Ut)/4)/2 + U$, corresponding to the localized density profile

$$\rho = \frac{M_0^2}{8} \operatorname{sech}^2\!\left(\frac{M_0(x - Ut)}{4}\right). \qquad (6)$$

The localization of bacteria in the band results from a competition between chemotactic attraction and diffusive smearing. The velocity U corresponds to an external attractant gradient across the band. However, in the experiments no external gradient is imposed, so this solution is inconsistent. (We note that in Keller and Segal's model of Adler's experiments (Adler, 1966), the above model also does not lead to moving bands (in that the cell density becomes negative!). Keller and Segal solved this dilemma by positing that the chemotactic coefficient k in Eq. 2 is a nonlinear function of the attractant concentration.)

Coupling to succinate

How can motion occur without an externally imposed attractant gradient? Note that unlike Adler's original experiments, in which bacteria create attractant gradients by consuming an attractant, in the present experiments the attractant is actually produced. To understand how motion can occur, it is necessary to consider the mode of attractant production. The attractant (aspartate) is produced by the enzyme aspartase from fumarate and ammonia:

$$\text{Succinate} \rightarrow \text{Fumarate} + \text{Ammonia} \rightarrow \text{Aspartate}. \qquad (7)$$

Presumably, cells exposed to succinate convert succinate to fumarate via the tricorboxyl acid cycle:

$$\text{Succinate} - \text{H}_2 \rightarrow \text{Fumarate}. \qquad (8)$$

Budrene and Berg (1995) have shown experimentally that the rate of aspartate production is determined by the concentration of exogenous succinate. This succinate is being exausted by the cells during the experiments. In the following, we will argue that it is the depletion of the succinate that is necessary for the attractant production that drives the motion of the ring.

The dynamical equations coupling the bacterial density, attractant, and succinate follow from the fact that the attractant production rate is a linear function of the succinate concentration. For local bacterial density ρ, the rate of aspartate production is $\tilde{\alpha}\rho f$, depending on the product of the bacterial density and the succinate concentration.

This modifies the attractant production (Eq. 4) and requires an additional dynamical equation for the succinate concentration. Under the assumptions outlined above about the relative time scales of the various physical processes, the full equations become

$$\partial_t \rho = \nabla^2 \rho - \nabla \cdot (\rho \nabla c) \qquad (9)$$

$$0 = \nabla^2 c + f\rho \qquad (10)$$

$$\partial_t f = -\gamma \rho + \beta \nabla^2 f, \qquad (11)$$

where we have nondimensionalized the equations using the same scales introduced above for the density and attractant concentration, as well as the concentration f_∞ of succinate on the plate. The dimensionless succinate consumption is

$$\gamma = \frac{rD_c}{f_\infty^2 \tilde{\alpha} k},\tag{12}$$

where r is the rate of succinate consumption and D_f is the diffusion constant for succinate. The parameter $\beta = D_f/D_b$ is a dimensionless measure of food diffusion.

The most important issue in understanding traveling bands is to understand what is actually driving the ring forward. There are two possibilities: 1) an imbalance of chemotactic fluxes, or 2) succinate consumption coupled with attractant production. We will see below that the subtleties of the bacterial response when the succinate is nearly exausted determine which of these two driving forces dominates. We will present two different models of the ring motion: the first model studies Eqs. 9–11. In a distinguished limit, the model can be solved exactly, and it will turn out that collective migration results from the fore-aft symmetry breaking caused by succinate consumption. Indeed, there are forward-moving solutions even when the bacteria in front of the band sense a negative gradient stronger than the positive gradient sensed by the bacteria behind the band.

The construction of a traveling band requires the matching of two different regimes: on the scale of the front, diffusion of attractant is fast (see above); far from the band diffusion, diffusion is slower. The matching of the solution for this model will present a paradox, that traveling solutions do not exist in steady state. In an effort to resolve the problem, we introduce a second model that takes into account the fact that when the succinate on the substrate is exausted, bacteria begin to consume aspartate.

Structure near the band

A traveling wave ansatz $\rho(x - Ut)$, $c(x - Ut)$, and $f(x - Ut)$ in Eqs. 8–10 reduces the solution in the regime near the front to the ordinary differential equations

$$-U\rho = \rho' - \rho c'\tag{13}$$

$$0 = c'' + f\rho\tag{14}$$

$$-Uf' = -\gamma\rho + \beta f''.\tag{15}$$

The imposed boundary conditions are that 1) the succinate concentration $f \to 1$ as $x \to \infty$; 2) the succinate concentration $f \to f_0$ as $x \to -\infty$, where f_0 is a constant to be determined; and 3) the bacterial density approaches zero far from the ring.

Before proceeding, let us comment on the approximation that has been made thus far. We have neglected the time derivative of the attractant concentration by arguing that it diffuses much faster than the bacteria. On the other hand,

we have not dropped the time derivative in the equation for the succinate. The reason for this is that, as we will see below, substantial analytical progress can be made when D_f is much smaller than D_b. In the limit where food diffusion is small ($\beta \ll 1$), the traveling wave solutions can be solved exactly. Although this limit does not directly apply to the experiments, these exact solutions considerably clarify how succinate coupling can cause ring motion. In the Appendix, we also consider the limit where $D_f \approx D_b$, and show numerically that the qualitative properties of the exact solutions for $\beta \ll 1$ are robust; in particular, the constraints of matching to the outer solution are identical. In a later section we consider a modified model for ring motion in which the correct limit is employed.

The analysis begins by defining $S = c'$, so that the second equation becomes $S' = -f\rho$. The equations can be solved exactly by considering ρ and S as functions of f instead of a function of x. This can be done with the transformation

$$\frac{d}{dx} = f'\frac{d}{df} = \frac{\gamma}{U}\rho\frac{d}{df},$$

where the second equality follows from Eq. 15 (with $\beta = 0$). Equations 13 and 14 become

$$\rho_f = \frac{U}{\gamma}(-U + S)\tag{16}$$

$$S_f = -\frac{U}{\gamma}f,\tag{17}$$

which can be integrated immediately to give

$$S = A - \frac{U}{2\gamma}f^2\tag{18}$$

$$\rho = B + U/\gamma(A - U)f - \frac{U^2}{6\gamma^2}f^3.\tag{19}$$

Imposing the boundary conditions that $\rho(f = f_0) = \rho(f = 1) = 0$ gives

$$B = -U^2/(6\gamma^2)(f_0 + f_0^2)$$

and

$$A = U + U/(6\gamma)(1 + f_0 + f_0^2).$$

The velocity of the solution can be related to the mass either by integrating Eq. 13 or just by computing

$$\int dx\,\rho = \int df\frac{\rho}{f'} = \frac{U(1 - f_0)}{\gamma} = M_0,$$

so

$$U = \frac{\gamma M_0}{1 - f_0}.\tag{20}$$

The complete profiles are

$$S(f) = \frac{M_0}{1 - f_0}\left[\left(\gamma + \frac{1 + f_0 + f_0^2}{6}\right) - \frac{f^2}{2}\right] \tag{21}$$

$$\rho(f) = \frac{M_0^2}{6(1 - f_0)^2}(1 - f)(f - f_0)(1 + f + f_0). \tag{22}$$

The solution has two free parameters, M_0 and f_0. The former is fixed by the number of bacteria in the ring; the latter is fixed by the condition that the attractant gradient behind the front $S(f_0)$ matches the attractant gradient far behind the moving front. This matching condition fixes f_0 behind the front, and thus the ring velocity.

Before considering the matching condition in more detail, we remark on qualitative features of these solutions. An interesting feature is that at small γ the ring moves forward, even when the attractant gradient in front of the band has a negative sign and is stronger than the gradient in back of the band! Thus the motion of the ring does not result from an imbalance in chemotactic fluxes on the two sides of the ring, but instead is a result of the effect of the depletion of succinate on the attractant production. As an example, when $f_0 = 0$ and $\gamma = 1/12$, the attractant profile is perfectly symmetrical, and the band still moves at velocity $U = M_0/12$. The role of the attractant gradient is to localize the bacteria in the band. The density profile is asymmetrical, however, regardless of the attractant distribution, because of the asymmetry in the succinate.

The spatial dependence follows from integrating $f' = \gamma/U\rho = \rho/M_0$ and using Eq. 22 for $\rho(f)$. As an example, if $f_0 = 0$, the solution is

$$f = \left(\frac{\exp M_0/6x}{2\cosh M_0/6x}\right)^{1/2}, \tag{23}$$

which implies the density profile

$$\rho = \frac{M_0^2}{6}\left(\frac{\exp - M_0/12x}{2\cosh M_0/6x^{3/2}}\right). \tag{24}$$

This profile is plotted in Fig. 1 and is valid for all nonzero γ. Note the asymmetry in the profile: the decay rate of the cell density on the trailing edge is slower than the decay rate on the leading edge. The attractant profile and succinate profile are also shown in Fig. 1 in the limit of small γ.

The profile differs from that in the front (Eq. 6) found above for the case where there is no food consumption, which is perfectly symmetrical.

Matching to outer solution

Now we consider matching to attractant gradients far from the front. This matching determines the value of f_0 and thus the velocity of the ring. At a distance $D_c/U \approx 3$ mm from the front, it is not valid to assume that the attractant diffusion is fast. Because D_c/U is much larger than the characteristic width of the band, in this regime the bacteria density
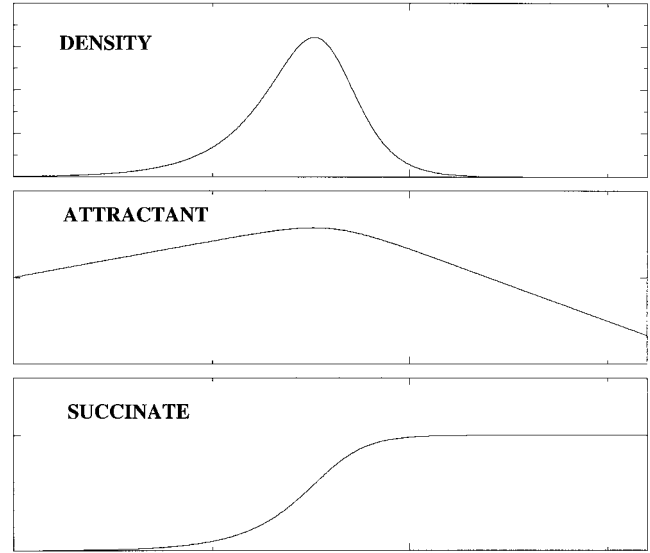

FIGURE 1 Traveling wave solution for the ring with $f_0 = 0$. The lowermost figure gives the succinate profile, the middle profile gives the attractant concentration, and the uppermost profile gives the density profile. All profiles are for $M_0 = 1$, in the limit of small γ.

essentially vanishes, and the succinate concentration is correspondingly constant. The equation for the concentration of attractant is

$$\partial_t c = \nabla^2 c + \rho(x - Ut)f(x - Ut) \tag{25}$$

where ρf is the source of attractant produced by the moving band of bacteria. On a length scale much larger than the width of the band, the attractant source can be approximated by $\rho(x - Ut)f(x - Ut) \rightarrow \beta\delta(x - Ut)$. The strength of the delta function $\beta = \int_{-\infty}^{\infty}\rho(y)f(y)dy = M_0(1 + f_0)/2$. The solution to Eq. 25 is

$$c(x, t) = \int dx_0 dt_0 \frac{\beta}{\sqrt{4\pi(t - t_0)}}\delta(x_0 - Ut_0)\exp\left[-\frac{(x - x_0)^2}{4(t - t_0)}\right]. \tag{26}$$

As $t \rightarrow \infty$, after the transients die out, the concentration approaches the steady-state solution,

$$c_{\text{outer}}(x, t) = \frac{M_0}{2U}(1 + f_0) \quad x < Ut \tag{27}$$

$$= \frac{M_0}{2U}(1 + f_0)e^{-Ux} \quad x > Ut.$$

This solution must be matched to the front solution constructed above. The matching condition is that attractant gradients $c'_{\text{outer}}(x)|_{x\rightarrow Ut_+} \rightarrow S(1)$, and $c'_{\text{outer}}(x)|_{x\rightarrow Ut_-} \rightarrow S(f_0)$, where $S(1)$ and $S(f_0)$ are the far-field attractant gradients from the inner solution in Eq. 21. Note that because the jump in attractant gradient across the front is the same in the inner and outer regions, the conditions on $S(1)$ and $S(f_0)$ are equivalent. This matching condition leads to the determination of f_0, and thus the velocity of the front.

We now proceed with the matching. Equation 27 implies that in steady state the matching condition is that $S(f_0) = 0$. Equation 21 implies that $f_0 = \frac{1}{4} \pm \sqrt{9/16 + 3\gamma}$. Neither of these solutions are in the physical range $0 \leq f_0 \leq 1$. Thus it is not possible to consistently match the two regimes!

The physical reason for this problem is that when the attractant gradient behind the front vanishes, there is nothing to keep the bacteria in back of the ring from diffusing away from the band. This difficulty is not a result of the approximations employed, but is an inherent problem arising from the fact that the steady-state profile of a moving band producing a constant amount of attractant per unit time has no attractant gradient behind the front. From formula 21 for the attractant profile in the band, the smallest attractant gradient that holds the traveling bands together occurs when $f_0 = 0$, where $S_{crit} = M_0(\gamma + 1/6)$.

How is this problem resolved?

1. One possibility is that the traveling band seen in the experiments is not in steady state. That is, there is insufficient time for the solution in Eq. 26 to approach steady state. The time it takes for convergence to c_{outer} depends on the boundary conditions on the attractant far behind the front. In the experiments, there must be sufficient time for the attractant production to fill up the entire interior of the swarm ring to the level dictated by the steady solution. Because the amount of time needed for attractant to diffuse across a typical swarm ring of radius 2 cm is on the order of 4×10^5 s and thus is already on the order of the total time of the experiment, it is implausible that a steady state is reached. Before the steady state is approached, there is a positive attractant gradient behind the band. As long as this gradient is larger than the critical gradient S_{crit}, the band will move forward. Of course, within this scenario, the ring motion is only a transient behavior. The reason the ring does not stop in the experiments is that a steady state is not achieved before the bacteria reach the end of the petri dish.

2. Another possible resolution is that the experiments are in steady state and attractant is degraded behind the front. When the succinate concentration is low, there is a natural mechanism for triggering aspartate consumption: namely, succinate serves as a carbon source for *E. coli* metabolism. When it is exausted, the only carbon source that is left for metabolic function is the attractant itself. Thus it is plausible that under conditions of low succinate, the bacteria consume aspartate. In other experimental situations (e.g., the original experiments of Adler, 1966), aspartate consumption is common. If such attractant consumption occurs, the rate of consumption would cause an attractant gradient behind the band. The strength of the gradient would be determined by the rate of degradation of attractant.

Steady bands with aspartate consumption

This mechanism of aspartate consumption is sufficiently plausible that we proceed to formulate a model for the structure of the band under this assumption. There is one additional experimental fact that is necessary: there is a time delay $\tau_{delay} \approx 20$ min after which a bacterium in a low succinate environment begins consuming aspartate. The reason for this is that aspartate consumption uses a chemical pathway different from that of succinate consumption, which requires a shift in the bacteria metabolism. (There is a subtlety of aspartate consumption that we are not going to treat here: namely, succinate serves primarily as a carbon source for *E. coli*. The bacteria also need nitrogen to function normally. The primary nitrogen source is ammonia salts, which are fixed in every experiment at the initial concentration of 3 mM. Eventually, of course, the ammonia will be consumed. It is known that under these conditions aspartate becomes a nitrogen source (Reitzer, 1996). Hence aspartate consumption is probably triggered in the experiments both by the depletion of the ammonia salts, as well as the depletion of succinate. We believe that the essential features of the model are the same in each case; because current experiments systematically vary succinate (and not ammonia), we focus only on this case.) The consequence of this time delay is that there is a region of size $\sqrt{D_b \tau_{delay}} \approx 1$ mm behind the band, where the succinate concentration is essentially constant and aspartate is not consumed. The size of this region is larger than the width of the band, which motivates dividing the solution into three regions: the front of the band, where attractant diffusion dominates; the back of the band, where attractant diffusion and consumption are balanced; and the region of the band. For reasons that will become clear, within this model it is possible to proceed analytically when the food diffusion constant is large (i.e., $D_f = D_c$, the physically appropriate limit).

The solution near the band obeys

$$-U\rho' = \rho'' - (\rho c')' \tag{28}$$

$$0 = c'' + f\rho \tag{29}$$

$$0 = f'' - \tilde{\gamma}\rho, \tag{30}$$

where $\tilde{\gamma} = (D_b D_c r)/(f_\infty^2 \alpha k D_f)$. When the band width is much narrower than the diffusive scale, the food equation decouples from the density and attractant equation. The succinate concentration is a constant f_0 across the band and increases to its initial value in front of the band. In this limit, both ρ and c reduce to the Burger's profiles constructed above! The solutions are

$$\rho_{inner} = \frac{M_0^2}{8} \operatorname{sech}^2\left(\frac{M_0(x - Ut)}{4}\right); \tag{31}$$

$$c_{inner} = -\frac{M_0 f_0}{2} \tanh(M_0(x - Ut)/4) + U \tag{32}$$

$$f'_{inner} = A + \frac{\tilde{\gamma} M_0}{2} \tanh(M_0(x - Ut)/4). \tag{33}$$

The free parameters in the solution are the mass per unit length M_0 of the ring, the succinate concentration f_0, the average succinate gradient A, and the ring velocity U.

In front of the band, the attractant (succinate) satisfies a diffusion equation with a source (sink), as in the previous subsection. The attractant concentration $c_{\text{front}} = Be^{-\text{Ux}}$, and the succinate concentration $f_{\text{front}} = 1 - \tilde{\gamma}M_0/Ue^{-\text{Ux}}$. In back of the band, the succinate concentration is constant, and the aspartate concentration is set by the balance of diffusion and consumption: the steady-state attractant profile c_{back} obeys $c''_{\text{back}} = \alpha c_{\text{back}}$, where α is the consumption rate (depending on both the rate of aspartate consumption and the number of bacteria that are consuming). The solution to this is $c_{\text{back}} = Be^{\sqrt{\alpha}\text{x}}$.

These three regimes must be matched to each other. Matching the attractant and succinate gradients of the back to the inner solution yields $A = \tilde{\gamma}M_0/2$ and $M_0 f_0/2 + U = B\sqrt{\alpha}$. Continuity of the succinate concentration across the front implies that

$$U = \tilde{\gamma}\frac{M_0}{1 - f_0}. \qquad (34)$$

Matching the solution in front of the band to the inner solution yields $-BU = -M_0 f_0/2 + U$. These equations can be solved simultaneously for B, U, and f_0. In the limit of slow food consumption $\tilde{\gamma} \ll 1$, the solution is $B = M_0 f_0/\sqrt{\alpha}$, $U = \tilde{\gamma}M_0/(1 - 2\tilde{\gamma})$, and $f_0 = 2\tilde{\gamma}$.

Comparison to experiments

To summarize, we have constructed two different models for traveling bands. The first solution uses succinate consumption to power the ring. Because of the fact that a band that produces a constant amount of attractant per unit time has no attractant gradient behind it in steady state, this solution is necessarily transient. The second solution gets around this difficulty by using the biochemical fact that at low succinate concentration, the bacteria consume aspartate to power a steady motion. For the reasons discussed above, on the basis of the present experiments, it is not possible to distinguish between these two models. Indeed, both solutions provide a biologically consistent mechanism for ring migration in the absence of an externally imposed gradient. Moreover, the qualitative properties of the both solutions match well with experiments. For example,

- The velocity of the swarm ring (formulae 20 and 34) decreases with increasing succinate concentration. This inverse relation between velocity and succinate concentration is also demonstrated by the experiments (Budrene and Berg, 1995). In the Fischer's equation model for ring motion, the ring velocity is independent of the substrate concentration (Murray, 1989; Tsimring et al., 1995).
- The velocity of the swarm ring increases linearly with the number density of bacteria in the ring. Thus the ring accelerates as it moves across the plate. Experiments verify this tendency (Budrene and Berg, 1995). (Another possible source for the acceleration of the band as it moves across the plate is effects of the curvature of the ring. If ℓ is the thickness of the band, and R is the radius

of the swarm ring, we expect these to contribute a correction of order $D/(Ur) \approx 0.01$ to the velocity. This is too small to explain the observed acceleration in the experiments (Budrene and Berg, 1995).)
- The characteristic thickness of the ring scales inversely with the cell density per unit length M_0 of the ring. As the ring moves across the dish, it will therefore sharpen; we have observed this qualitatively in the experiments, although quantitive measures have not yet been carried out.

Relation to Keller-Segal bands

It is interesting to contrast the swarm ring solutions presented here with those constructed by Keller and Segal (1970) to describe the original bands of Adler (1966). The crucial difference between the Adler bands and those in the present experiments is that in Adler's experiments the bacteria consumed attractant, whereas in the present experiments the bacteria consume a reactant for the production of attractant. In constructing a traveling solution for a bacterial band driven by attractant consumption, Keller and Segal also arrived at the dilemma discussed above (Keller and Segel, 1970; Keller and Odell, 1975) that there are no traveling solutions to Eqs. 1 and 2 (with positive bacterial density) without an external attractant gradient. Their approach to resolving the dilemma differs from that presented here: they introduced a nonlinearity in the chemotactic response coefficient k in Eq. 1. They found that for traveling solutions to the basic chemotactic Eqs. 1 and 2 to exist, it was necessary that the chemotactic response coefficient k diverge with vanishing attractant concentration. Physically, steady ring motion requires that the bacteria in regions with very small attractant respond quickly. Otherwise, if this assumption is not fulfilled, a nonsteady "diffusive" tail of bacteria is left behind the front.

Experiments on the chemotactic response of *E. coli* have subsequently demonstrated that this assumption about the chemotactic response is invalid. Impulse response experiments by Berg and collaborators (Segall et al., 1986; Berg, 1988) measure the chemotactic constant directly, and find no dramatic increase in chemotaxis as the attractant concentration vanishes.

The present study gives another mechanism that may cause the ring to move. In the context of the Budrene-Berg experiments, the mechanism requires 1) the existence of another external field that the bacteria consume and 2) that the rate of attractant production depend on the concentration of the additional field. This mechanism can also be generalized to encompass Adler's experiments, in which the bacteria consume the attractant instead of producing it. In this case we again require the presence of an additional field, and that the rate of attractant consumption decreases with increasing concentration of the additional field. As a simple model for how this might work, we let h denote the concentration of an additional (nonchemotactic) field. The

equations for a traveling band are then

$$-U\rho = \rho' - c'\rho \tag{35}$$

$$0 = c'' - F[h]\rho \tag{36}$$

$$-Uh' = -\gamma\rho + \beta h'', \tag{37}$$

where $F[h]$ reflects how the consumption of the attractant c depends on the presence of the field h. An approximate form for $F[h]$ might be $F[h] = 1 - \alpha h$. In the $\beta = 0$ limit, the equations can again be solved exactly. The solutions demonstrate that localized traveling rings exist whenever the nonlinearity coupling h to the attractant depletion is strong enough: $\alpha > 3\gamma$.

There is some evidence for this type of mechanism in the Adler experiments. Adler (1966) studies migrating bands both in capillary tubes and in agar plates. In all experiments cited, bands only form when there are two or more consumable chemicals that are interacting, which is consistent with the above mechanism. The only experiment Adler mentions that has only one active chemical (galactose) shows no rings. (Adler also does experiments with only oxygen, which show the formation of rings. However, he states that these rings "oxidize an endogenous energy source known to be present." Thus there is another active chemical for the oxygen rings.) The complication in interpreting Adler's experiments is that generally the bacteria are chemotactic toward more than one of the chemicals that are being consumed. Thus the analog of the attractant field c in the above equations would be a linear combination of the concentrations of the various chemicals toward which the bacteria are chemotactic. More work along these lines is necessary.

AGGREGATE FORMATION

The other major structure appearing in the experiments are aggregates. The fundamental feature of aggregate formation is that they form on a much faster time scale than the motion of the ring. Whereas the swarm ring moves across the petri dish in about a day, aggregate formation occurs in several minutes. The theory of aggregate formation is based on the fact that the chemotactic Eqs. 3 and 4 have solutions that form finite time singularities, with the bacterial density diverging. These solutions exist in both two and three dimensions. Two-dimensional collapse corresponds to a cylindrical mass of bacteria contracting to a line; three-dimensional collapse corresponds to a spherical mass of bacteria contracting to a point. Note that one-dimensional collapse, in which a mass of bacteria collapses to a two-dimensional plane in finite time, cannot happen; this is because the one-dimensional chemotactic equations are equivalent to Burger's equation, for which singular solutions do not exist. The physical mechanism for the singularities is that the accumulation of bacteria increases the attractant production, which further increases the bacterial density. The fact that chemotactic equations can admit singular solutions was

argued long ago by Nanjudiah (1973), and elaborated in the definitive paper of Childress and Percus (Childress and Percus, 1981; Childress, 1984), who dubbed this phenomenon "chemotactic collapse." Recent studies have examined chemotaxis collapse in generalized mathematical models (Raschle and Ziti, 1995).

We now discuss the structure of the collapsing solution. During the initial stages of aggregation, the depletion of succinate is unimportant. Succinate consumption occurs on a time scale γ^{-1}, whereas aggregate formation is singular and thus happens faster. Close enough to the collapse point, the high bacterial densities will cause the depletion of all of the oxygen near the aggregate, which will stop bacterial motion and chemotactic aggregation (Anderson and von Meyenburg, 1980; Adler and Templeton, 1967). This effect is considered in detail below.

To start, we consider the coupled Eqs. 3 and 4. To study the time dynamics of the singular solutions, we take the three-parameter family of initial conditions,

$$\rho(r, t = 0) = \frac{2(p - 1)Na^{p-1}}{(a + r^2)^p}, \tag{38}$$

and numerically solve the "radially symmetrical" versions of Eqs. 3 and 4 by using a standard implicit finite-difference scheme with adaptive mesh refinement. In two dimensions, the parameter N is the total number of bacteria. Figure 2 shows the bacterial density for a case where a singularity occurs ($N = 50$, $p = 4$, $a = 1$). The initial profile quickly develops a singularity at the origin. The inset shows the dependence of the maximum bacterial density as a function of the characteristic width L of the collapsing region, which obeys the scaling law $\rho(0) \approx L^{-2}$.
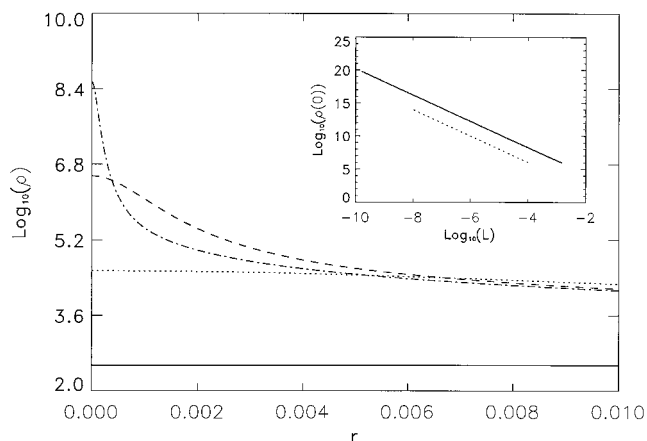

FIGURE 2 Numerical simulations of the finite time singularity in the bacteria density. The solid, dotted, dashed, and dot-dashed lines correspond to $t = 0$, $t = 7.69 \times 10^{-4}$, $t = 7.89 \times 10^{-4}$, and $t = 7.90 \times 10^{-4}$, respectively. The inset shows the maximum density versus characteristic width of the singularity (*solid line*), as well as the scaling law $\rho(0) \approx L^{-2}$ (*dotted line*).

The entire singularity is described by a similar solution of Eqs. 3 and 4, of the form

$$\rho(r, t) = L^{-2}R(rL^{-1}) \qquad (39)$$

$$c(r, t) = S(rL^{-1}). \qquad (40)$$

The characteristic scale L has the time dependence $L \approx (t^* - t)^{1/2}$, up to logarithmic corrections. The logarithmic corrections are an interesting mathematical property of the solutions (Herrero and Velazquez, 1996; S. C. Venkataramani et al., unpublished manuscript) and will be discussed in a subsequent publication. We remark that (modulo the logarithms) the same scaling laws are observed in our simulations for both two-dimensional collapse and three-dimensional collapse.

Extensive numerical simulations show that the occurrence of collapse into dense aggregates depends strongly on the number of bacteria in the initial cluster, but only weakly on the parameters a and p in the initial conditions above. For N below the "Chandrasekhar limit" N^*, the bacteria decay to a uniform state. Above N^* singularities always form. In two dimensions, $N^* = 4$ in dimensionless units; in three dimensions the critical mass depends on the system size (S. C. Venkataramani et al., unpublished manuscript). The existence of a critical N in two dimensions was originally noted by Childress and Percus (1981) and Childress (1984).

For the present experiments, the critical number in two dimensions is

$$N^*(2D) = \frac{4D_bD_c}{k\alpha}, \qquad (41)$$

where the parameters are defined in Eq. 1. Measurements of D_b and k have been made by Berg and Turner (1990) for swimming in a liquid medium. Their experiment consists of two closed cells joined by a 0.05-cm permeable plate. By controlling the relative attractant concentrations in the two cells, and counting the number of bacteria migrating from one cell to the other, it is possible to extract both D_b and k. Berg and Turner report that $D_b = 6.6 \times 10^{-6}$ cm²/s. From Figure 4 of their paper, we have extracted the chemotactic coefficient $k = 10^{-14}$ cm⁵/s. Both of these numbers are consistent with expectations: the diffusion constant $D_b = \ell v$, where ℓ ($\approx 30 \mu$) is the typical run length and v (≈ 30 μm/s) is the swimming velocity (Berg, 1988). The chemotactic coefficient can be similarly expressed as $k = c\ell^4v$, where the constant c represents the strength of the chemotactic response. The attractant production rate $\alpha \approx 10^3$ molecules/s/bacteria (Budrene and Berg, 1995). Putting these numbers together implies that in a liquid medium, $N^*(2D: \text{liquid}) \approx 10^3$/cm. Most of the experiments discussed in this paper take place in agar. Here it is known (Wolfe and Berg, 1989) that obstructions in the agar shorten the characteristic run length ℓ, leading to a dramatic decrease in both k and D_b. The critical number in agar is

$$N^*(2D: \text{agar}) \approx 10^3/\text{cm} \frac{1}{\ell_{\text{agar}}^3},$$

where ℓ_{agar} is the run length in agar. A 10-fold decrease in the run length leads to a 1000-fold increase in N^*.

There are several strong experimental indications that the aggregates in the Budrene-Berg experiments indeed represent chemotactic collapse:

- First, the time scale for aggregate formation is much faster than any other experimental time scale, a hallmark of singularities.
- A second experimental indication that chemotactic collapse is occurring comes from experiments in which the bacteria are homogeneously distributed in a liquid medium (see Budrene and Berg, 1991). In this case, the bacteria are much more mobile, and in a short time (3–5 min) the medium is filled with three-dimensional aggregates. Experiments demonstrate that the number of aggregates scales linearly with the initial number of bacteria over a wide range of cell densities. For the initial bacterial densities 10^7, 10^6, and 2×10^5 cells/ml, the number of final aggregates was counted to be 287, 33, and 6, respectively; as predicted, a 10-fold (fivefold) decrease in the bacteria density leads to a 10-fold (fivefold) decrease in the number of aggregates. At much higher bacterial concentrations than 10^7 cells/ml, the process of secondary merges of initial aggregates occurs too rapidly to accurately count the number of aggregates. These experiments were performed with a thin layer of liquid covering a petri dish. More quantitative interpretations of these experiments are discussed in Appendix 3.
- Another (visual) indication of singular collapse is shown in Fig. 3. The aggregation produces very densely packed structures, with a density so high in the center of the aggregate that light cannot penetrate through the layer.

Of course, in the actual experiments the aggregation singularity does not proceed until the bacterial density is infinite. What stops the singularity? We first note that because the attractant concentration c does not diverge at the collapse point, the saturation of the chemotactic response at high attractant concentration (Dahlquist et al., 1972) cannot stop the collapse. Correspondingly, we also note that bacterial division does not modify the collapse because the rate of division $a\rho \approx a(t^* - t)^{-1}$ is asymptotically smaller than $\partial_t\rho \approx (t^* - t)^{-2}$ when $t \rightarrow t^*$.

There are essentially three possibilities for stopping the collapse:

1. Nonlinearities in the cell division rate can stop the collapse as long as they are strong enough. For a cell division rate $a\rho(a - b\rho)$, the nonlinearity $\approx \rho^2 \approx \partial_t\rho$ when $\rho \approx (t^* - t)^{-1}$. Thus if b is high enough, we expect this to arrest the collapse. This effect is apparently observed in the simulations of Tyson et al. (1997).
2. Another possibility is depletion of succinate, which would halt (and indeed eventually reverse) attractant production. Because $\partial_t f \approx -\rho \approx (t^* - t)^{-1}$, the succinate will vanish after a finite time. When this occurs, the bacteria will continue to migrate up the attractant gradi-
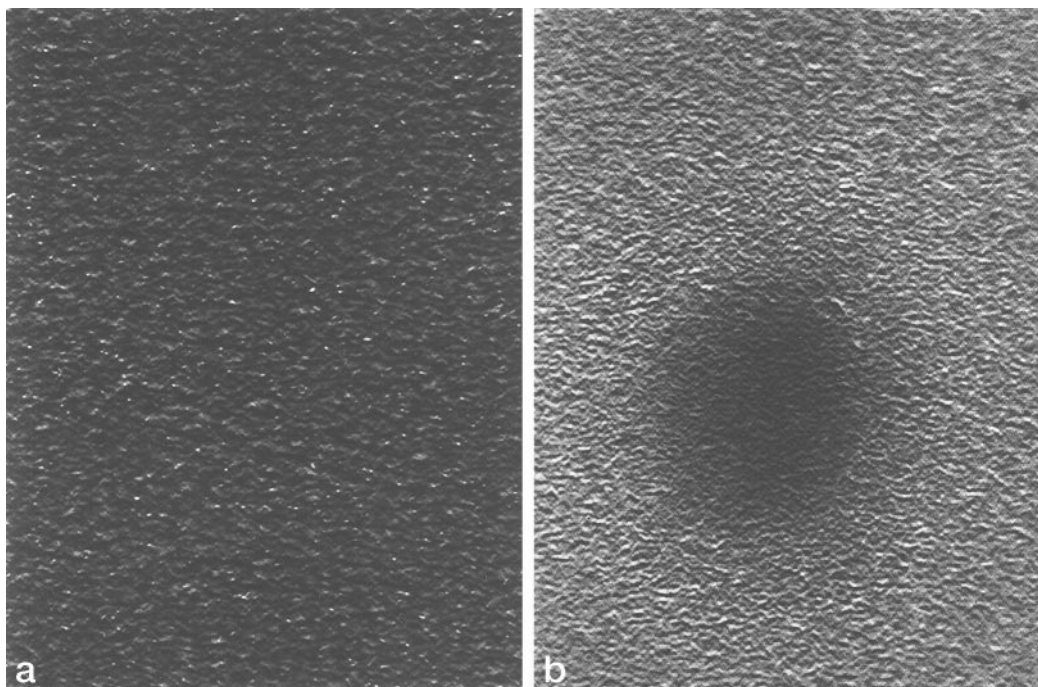
FIGURE 3 (*A*) Bacterial distribution far from an aggregate in a growing colony, obtained by phase-contrast light microscopy. White dots represent the bacteria. (*B*) Densely packed bacteria in an aggregate. The central dark spot represents such extreme local cell density that light does not penetrate the layer. The bright halo around the central spot corresponds to intermediate densities. Colonies were grown as in Budrene and Berg (1991).

ent already produced, although the gradient will not steepen further.

3. The effect that we believe is most relevant for stopping collapse is oxygen depletion. It has been shown (Khan and Macnab, 1980; Anderson and von Meyenburg, 1980) that exausting oxygen causes the bacteria to become immobile immediately. The fact that present experiments (Budrene and Berg, 1995) find that the collapse leaves a residue of immobile bacteria gives strong support to this mechanism.

At what bacteria density is oxygen depleted?

The dynamics of oxygen X is described with a diffusion equation with depletion caused by bacterial density:

$$\partial_t X = D_{oxygen} \nabla^2 X - \beta \rho.$$

Using the similarity solution for the collapsing aggregate gives

$$\partial_t X \approx -\beta \frac{1}{L^2} F\left(\frac{r}{L}\right),$$

or $X \approx X_\infty + \beta \log(t^* - t)$, where X_∞ is the oxygen concentration away from an aggregate. This implies that the oxygen is depleted a time $t^* - t \approx \exp(-X_\infty/\beta)$ before the collapse singularity. The fact that the maximum density of the collapsing solution scales like $(t^* - t)^{-1}$ implies that the maximum bacterial density in the aggregates ρ_{max} is on the

order of

$$\rho_{max} \sim \exp\left(\frac{X_\infty}{\beta}\right). \tag{42}$$

As X_∞ increases, the maximum density increases exponentially within the aggregates, so that a twofold increase in oxygen density leads to an e^2 increase in the maximum bacterial density. This relationship has not yet been tested in experiments. Because the oxygen concentration in the petri dish is set by the atmospheric pressure, we hope to test it in the future by studying the aggregate densities as a function of the overhead oxygen pressure in a closed vessel. Presumably, if the oxygen concentration is high enough, ρ_{max} will approach the "hard packing" limit of the bacteria.

COLLAPSING INSTABILITY OF A SWARM RING

To complete our picture of the experiments, it is necessary to understand how the swarm ring destabilizes into aggregates. A natural possibility for how this might happen is via a linear instability of the ring, namely, modulating the bacterial density along the ring causes more attractant to be produced where the bacterial density is highest. The enhanced attractant concentration will cause bacteria to flow toward this region, enhancing the concentration even further. This instability mechanism is well known to operate in other situations. For example, during the streaming instability of *D. discoideum*, fluctuations in the local cell density produce fluctuations in the cAMP production, with chemo-

taxis toward regions of higher concentrations (Bonner, 1967; Lee et al., 1996; Hofer and Maini, 1997; Kessler and Levine, 1993; B. N. Vasiev et al., 1994; Hofer et al., 1995).

For the present experiments, this instability argument is both conceptually appealing and straightforward to demonstrate mathematically. Appendix 2 analyzes the stability of the inner region of the traveling bands constructed above and demonstrates the existence of a linear instability. This corroborates the results of all computer simulations to date of the Budrene-Berg experiments (Bruno, 1992; Woodward et al., 1995; Ben-Jacob et al., 1995; Tsimring et al., 1995; Tyson, 1996; Tyson et al., unpublished manuscript), which exhibit (one-dimensional) traveling rings destabilizing via transverse instability into spots of bacteria. The fact that these different computer simulations assume different dynamics (agreeing to varying degrees with that proposed here) implies that this instability mechanism is robust.

However, as is emphasized in both the preceding section and in Appendix 3, there is more to aggregate formation than just a linear instability. In fact, Appendix 3 demonstrates that there are both qualitative and quantitative discrepancies between what is expected from strongly nonlinear events (and what is actually observed in experiments) and what would be expected from a purely linear instability.

To illustrate this point, consider the destabilization of the swarm rings in a hypothetical two-dimensional experiment: the linear instability of Appendix 2 predicts a most unstable wavelength c/M_0, where M_0 is the number of bacteria per unit length of the ring. Hence linear theory predicts that will be on the order of c bacteria per aggregate. The nonlinear threshold for aggregate formation is logically independent of this number. For this model, the number of bacterial aggregates formed from the linear instability exceeds the nonlinear threshold.

In the experiments, despite the appearance of a two-dimensional plate, the aggregates are actually three-dimensional objects. The plate thickness is small (≈ 0.5 mm) but finite. (In *D. dictostelium* experiments, the cells are a monolayer on the agar surface, in contrast to the situation here, where the bacteria uniformly fill the agar plate (before the instabilities).) Before aggregates form, the bacterial density is uniform across the plate thickness. As in the two-dimensional example discussed above, there is a critical threshold for aggregate formation in three dimensions; that in 3D depends on the size of the box in which the aggregate is confined (Brenner et al., 1997). Hence we expect an interplay between linear and nonlinear instabilities.

The sequence of events that actually occur in the experiments presumably depends on an interplay between the initial number of bacteria placed on the petri dish (and hence the number density in the swarm ring) and the values of the parameters (D_b, k, D_c, α) and biochemical effects (above). At present, all we can do is admit that there are a number of theoretical possibilities, and then give evidence for possible causes of what seems to occur in the experiments. The possible causes are:

1. The ring is linearly unstable (as computed in Appendix 2) and breaks directly into aggregates. This scenario is the one that is demonstrated by all computer simulations carried out to date. However, as implied above, there is serious reason to question those results, on the basis of the validity of the assumed biochemical effects, and even on the basis of the two-dimensionality of the simulations. Experiments are three-dimensional, and there are solid theoretical reasons to believe the difference between two and three dimensions is crucial.

2. Despite our calculation, the ring is linearly stable. This could happen if we neglected important biochemical effects in our model of the swarm ring, or if the interplay between the outer and inner solutions neglected in our stability analysis played an important role. In this scenario, the instability of the swarm ring is a nonlinear effect. That is, as the ring expands the number of bacteria multiply. Because if M is the mass per unit length of the ring, then

$$\dot{M} = aM - \frac{U}{r} M, \qquad (43)$$

where a is the reproduction rate, r is the radius of the ring, and U is the velocity. The mass of the band as a function of the distance from the center of the dish follows from approximating $\dot{M} \approx U\partial_r M$ and using $U = \gamma M/(1 - f_0)$. This gives the solution to Eq. 43 as

$$M(r) = \frac{(1 - f_0)a}{2\gamma} r + Cr^{-1}, \qquad (44)$$

When $M(r)$ exceeds the critical limit for collapse, the ring will collapse into a cylinder (which will subsequently destabilize into aggregates). A sketch of this possibility is shown in Fig. 4. From the top view, the ring is one-dimensional, but because of the finite thickness of the petri dish, a side view shows there is a three-dimensional structure. Note that because $M(r)$ is only a linear function of r,
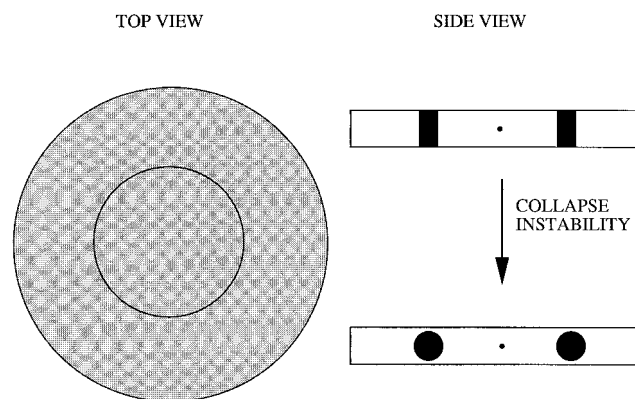

FIGURE 4   Sketch of instability of the swarm ring in a petri dish. The figure on the right shows a top view of the dish, with the circle depicting the swarm ring. The figures on the right denote a side view (including the finite thickness of the dish). The upper figure depicts the swarm ring before the instability, and the lower figure depicts the collapse of the ring into a cylinder.

the number of bacteria in the ring increases only by a factor of 10 in the course of the experiments, so this scenario requires that the number of bacteria in the initial swarm ring is close to the critical number.

3. Another possibility is that the ring is stable, and the formation of aggregates proceeds when the system directly crosses the nonlinear threshold for 3D aggregate formation (avoiding the cylinder stage entirely).

4. Finally, the ring could be linear unstable (as calculated in Appendix 2), but aggregate formation still could not happen until a nonlinear threshold is crossed. Within this scenario, aggregate formation could happen via either route 2 or route 3. The result of the linear instability would be that the density in the ring is time dependent, with modulations in the density in the direction transverse to the ring, even during the (seemingly) steady forward propagation stage.

On the basis of theory alone, it is not currently possible to distinguish these scenarios. It is even possible that the scenario that occurs depends on details of experiments that have not been systematically controlled. What do the experiments say? Figure 5 shows a photograph of a swarm

ring both immediately before and immediately after it starts to become unstable. It is seen that the ring is initially rather diffuse, and then undergoes a transition to a cylindrical shape, as described in Fig. 4.

The collapsing cylinder undergoes secondary instabilities to the formation of aggregates. The mechanism for the secondary instability is that density inhomogeneities in the collapsing cylinder cause an increase in the attractant concentration where the density is highest. This results in attractant gradients along the axis of the cylinder, which cause transverse flows of bacteria. The transverse flows cause the cylinder to break into three-dimensional aggregates.

How far does the swarm ring have to travel from the center of the dish before it destabilizes? Using formula 44 for the mass of the band as a function of the distance from the center of the dish gives $M(r) \approx ar/\gamma$ at large radii. The instability occurs when the mass per unit length exceeds the critical mass N^* for collapse, which happens at a radial distance r^* from the origin, where

$$r^* \approx N^*\gamma \approx \frac{1}{f_\infty^2}. \tag{45}$$

At low enough succinate concentrations, the critical radius is larger than the size of the petri dish, so that the instability does not occur. At high concentrations of succinate, the ring moves more slowly, but the doubling time of bacteria remains constant. Thus enough mass for collapse accumulates at a smaller radius.

This dependence of r^* on food concentration (Fig. 6) agrees with experiments; as an illustration we show the critical radius r^* plotted against the thickness h of the agar layer for a fixed amount of food in the dish. The three-dimensional food concentration f_∞^{3D} is held fixed in the experiments. The two-dimensional food concentration f_∞ is related to the three-dimensional one by $f_\infty = h f_\infty^{3D}$, so that increasing h at fixed f_∞^{3D} is equivalent to increasing f_∞. As predicted, the swarm ring radius decreases with increasing f_∞.

The number of bacteria per unit length of the ring when the instability occurs is predicted to be that given in Eq. 41. As stated above, the exact number depends on knowing the diffusion and chemotactic constants for migration in agar,
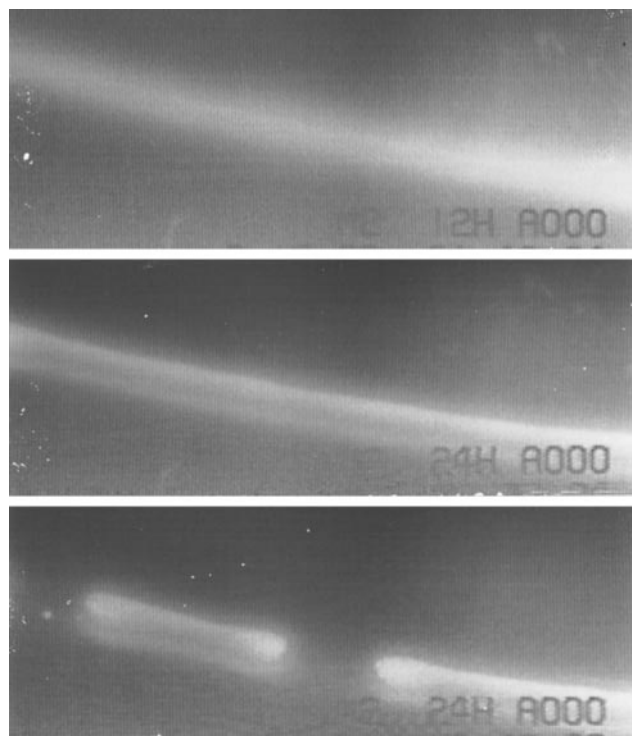

FIGURE 5   Structure of the swarm ring (magnified view) immediately before and after collapse visualized by scattered light. From top to bottom: Before collapse a traveling swarm ring looks like a dense band of cells, which transforms into a cylindrical structure that further collapses into aggregates. The time intervals between the first and the second pairs of pictures were 6 min and 3 min, respectively. A colony of *E. coli* HCB 317 was grown on 2 mM succinate (see Budrene and Berg, 1991). The frames are from a time-lapse recording made with a Hamamatsu model XC-77 CCD camera on a JVC model BR-9000U cassette recorder and were printed with a Sony model UP-870MD video printer. The recording was made against a flat-black background with illumination slantwise from below (see Budrene and Berg, 1991).
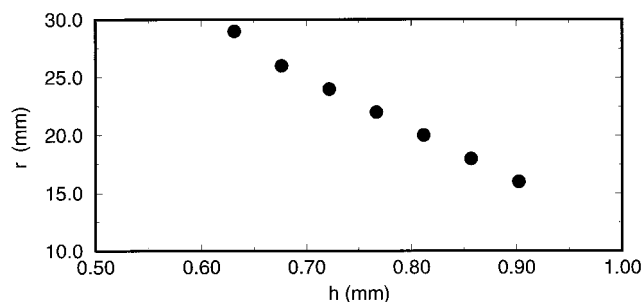

FIGURE 6   Measurements of the critical radius r^* as a function of the thickness of the agar layer, for fixed food concentration.

which are not known exactly. However, assuming that the run length decreases by a factor of 5 (a conservative estimate based on Figure 2 of Wolfe and Berg, 1989) gives $N^* \approx 10^5$ cm^{-1}. This estimate is quite reasonable in view of the experiments.

Finally, we remark that these experiments demonstrate that the instability is either via scenario (2) or (4) outlined above. In particular, we cannot rule out or rule in (from either experiments or theory) the presence of time-dependent structures in the band before the collapse. This topic is left to a future investigation.

CONCLUSIONS

This paper represents the first attempt to define a model of the Budrene-Berg bacteria experiments by combining chemotaxis with known biochemical processes operating between the cells and their environment. We have presented a theory of the basic structures observed in bacterial pattern formation, swarm ring migration, and aggregate formation. Our description is based on two simple ideas. 1) Swarm ring migration is caused by the depletion of a chemical used in the process of attractant production. A steady swarm ring requires attractant depletion far behind the front. In general, solutions for swarm rings can exist whenever the rate of production (or depletion) of a chemotactic chemical depends on the concentration of another external field. 2) Aggregate formation, as well as the instability of the swarm ring, results from the singular collapse of a cloud of bacteria into more compact structures of lower dimensionality. Collapse into a spatial point is the basic mechanism for aggregate formation; cylindrical collapse into a line is the mechanism for swarm ring instability.

The mechanism for swarm ring migration by coupling to two external fields (one of which is chemotactic) allows the bacteria to migrate in the absence of externally imposed gradients. A single motile bacterium without chemotaxis due to the absence of external gradients of attractant would reach the edge of the agar plate in 100 days. The present mechanism explains the observed migration in ~40 h. Our mechanism differs from previous models of ring motion. Essentially two other mechanisms have been proposed: 1) The study of Keller and Segal (1970) ascribes ring motion to a nonlinear chemotactic coefficient that diverges with vanishing attractant concentration. 2) The other popular mechanism used in previous studies of the Budrene-Berg experiments (Tsimring et al., 1995) attributes the collective motion to a "Fischer's equation"-like mechanism, in which the motion is triggered by a competition between cell division and the competition of individual bacteria for food. The present theory ascribes motion to the consumption of succinate, the concentration of which limits the rate of attractant production. We believe that the experimental data provide strong support for our mechanism: impulse-response experiments on single bacteria (Segall et al., 1986; Berg, 1988) have demonstrated that the divergence of the chemo-

tactic coefficient with vanishing attractant concentration does not occur, which rules out the first mechanism for migration. The Fischer's equation mechanism implies that the front velocity is independent of the substrate concentration and of the total number of bacteria in the ring; the mechanism presented here predicts both a decrease in the front velocity with increasing substrate concentration and an increase in the front velocity with increasing numbers of bacteria. Both of these features are observed in experiments.

The mechanism for instability and breakdown into aggregates also differs from previous studies. All previous work (Bruno, 1992; Woodward et al., 1995; Tsimring et al., 1995; Ben-Jacob et al., 1995) has modeled the Budrene-Berg experiments with dynamical equations in two spatial dimensions, neglecting the finite thickness of the petri dish. In these models, the breakdown of the swarm rings arises because of "Turing-like" linear instabilities (Turing, 1952; Murray, 1989). In contrast, the present work shows that the instabilities of the swarm ring are inherently three-dimensional. The initial instability involves a transition in which the bacterial density becomes nonuniform in the direction perpendicular to the agar plate. A secondary instability causes the breakdown into aggregates. Although there are still serious issues remaining in understanding the instability mechanism, it seems clear that the most important physical mechanism is chemotactic collapse (Nanjudiah, 1973; Childress and Percus, 1981), which provides a unifying element among the various physical processes (aggregate formation and the instability of the swarm ring).

Turing's mechanism has been applied to many instances of biological pattern formation and remains the only theoretical model for understanding patterns in biological systems. There is an important conceptual and practical difference between Turing's instability mechanism and an instability mechanism mediated by chemotactic collapse. Turing mechanisms are based on linear instabilities, which are inherently not robust. Changes in the relative diffusion constants or consumption rates of the various species can both alter the instability threshold and change the characteristics of the final pattern. The addition of different reactive chemicals or other physical processes that happen on the time scale of the instability can have substantial effects on the final outcome. In contrast, the instability and breakdown into aggregates occurs because of highly nonlinear singularities in the chemotactic equations, in which bacterial densities and chemotactic fluxes diverge. The divergence of the chemotactic fluxes means that this dynamical event is robust. Changes in the chemical diffusion constants and consumption rates will not change the structure of the collapsing solution. Collapse will exist as long as the bacteria produce attractant. It is quite possible that in other instances of biological pattern formation, singular events play a key role.

An important consequence of the inherent robustness of the singularities in the present study is that we expect the features of the pattern formation involving chemotactic collapse to also apply to other species of bacteria that

produce attractant. For example, *Salmonella* (Woodward et al., 1995) excreting attractant also exhibit bands and aggregate formation. Although the properties of the bands are different in the *Salmonella* from those in the *E. coli* experiments discussed here (e.g., in contrast to the situation here, bands in *Salmonella* do not move), we expect the breakup of the bands to be via the same singular mechanism as for *E. coli*.

Finally, our analysis predicts a number of scaling laws, many of which were shown to be consistent with experiments. Several predictions remain to be tested. Probably the most interesting are the time dependences of the collapse singularity. During a collapse, the bacterial densities change by several orders of magnitude, which should be more than sufficient to verify the temporal scaling laws for the collapse singularity. For the swarm ring, it would be interesting to measure the profiles of the attractant and succinate concentrations around the swarm ring and test whether they agree with the present predictions.

APPENDIX A: TRAVELING BANDS AND FOOD DIFFUSION

This appendix discusses solutions to the traveling wave equations

$$-U\rho = \rho' - \rho c' \qquad (A1)$$

$$0 = c'' + f\rho \qquad (A2)$$

$$-Uf' = -\gamma\rho + \beta f'' \qquad (A3)$$

with nonzero β. As in the construction of traveling solutions above, we require the boundary conditions that $\rho \rightarrow 0, f \rightarrow 1$ as $x \rightarrow \infty$, and $f \rightarrow f_0$ as $x \rightarrow -\infty$. First we note that integrating Eq. A3 over the entire profile and applying the boundary conditions implies the relation $U = \gamma M/(1 - f_0)$ between the front velocity U and the mass per unit length M of the ring. This relationship holds regardless of the value of β. To find the spatial profiles, the equations must be integrated numerically. The presence of nonzero β means that the food Eq. A3 has an exponentially growing mode $f \approx e^{-Ux}$ as $x \rightarrow -\infty$, which corresponds to an additional condition on the solutions. However, the solutions also have an additional degree of freedom in satisfying this boundary condition, because nonzero β increases the order of the ODEs.

How many free parameters are there in satisfying these boundary conditions? We take $x = 0$, where $\rho'(0) = 0$ implies $c'(0) = U$. The constants $\rho(0), f(0)$, and $f'(0)$, as well as the velocity U are free parameters. For each $\rho(0), f(0), f'(0)$, the velocity U must be chosen so that the food concentration f does not grow at $-\infty$ (zeroing the exponentially growing mode mentioned above). This leaves three parameters, which can be tuned to adjust $f_\infty, f_{-\infty}$, and the total number of bacteria M_0 as desired. In this respect, the solutions with food diffusion are qualitatively similar to the solutions without food diffusion. Figure 7 shows the solution with $\beta = 1$, $M_0 = 4.15, \gamma = 1$.

APPENDIX B: STABILITY OF TRAVELING BAND

This appendix considers the stability of a propagating band to sinusoidal modulations. We consider the second model of the swarm ring (as formulated in the text) and examine the response of the band to perturbations in the neighborhood of the band. In this calculation, we do not consider the response of the perturbations on the solution far from the band (where attractant diffusion or succinate consumption might dominate), but instead simply examine the stability of the "Burger's inner region."
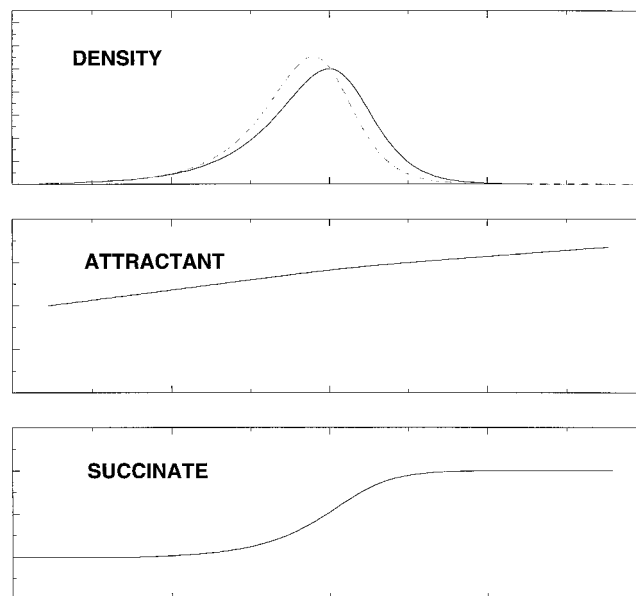

FIGURE 7 Traveling wave solution for the ring, with $\beta = 1$. The uppermost figure gives the density profile, the middle profile gives the attractant concentration, and the lowermost profile gives the succinate profile. All profiles are for $M_0 = 4.15$ and $\gamma = 1$. The dotted curve in the uppermost figure is the density profile for $\beta = 0$ with the same values of M_0 and γ. Although quantitative features differ, qualitative features are robust.

It was remarked in the text that the separation of scales between the thickness of the band and the diffusive scale decouples the succinate dynamics from the band dynamics. In this limit, the dynamics is governed by the equations

$$\partial_t\rho = \nabla^2\rho - \nabla \cdot (\rho\nabla c) \qquad (B1)$$

$$0 = \nabla^2 c + \rho. \qquad (B2)$$

These equations are equivalent to Burger's equation in one dimension under the transformation $v = \nabla c$. This equivalence implies that the equations have an important symmetry. Given a solution $\rho_0(x, y), c_0(x, y), \rho = \rho_0(x - Ut, y), c = c_0(x - Ut, y) - Ux$ is also a solution. This symmetry corresponds to Galilean invariance in the Burger equation.

The importance of this symmetry is that it implies that the stability of a traveling wave solution (within this approximation) is independent of the ring velocity. Thus we can consider the stability of a stationary solution ρ_0, c_0. The stability analysis begins by writing

$$\rho = \rho_0 + Fe^{\omega t}\cos(qy) \qquad (B3)$$

$$c = c_0 + Ge^{\omega t}\cos(qy). \qquad (B4)$$

Linearizing Eqs. B1 and B2 gives the two ordinary differential equations

$$\omega F = F'' - q^2 F - \rho_0' G' + 2F\rho_0 - c_0' F' \qquad (B5)$$

$$G'' - q^2 G = -F. \qquad (B6)$$

This is an eigenvalue problem for ω. We are interested in the stability for perturbations with wavelengths much larger than the thickness of the band. In this limit, it is legitimate to approximate the functional forms of ρ_0 and

c_0 as

$$\rho_0 = M_0 \delta(x) \tag{B7}$$

$$c_0' = -M_0 \theta(x) + \frac{M_0}{2} \tag{B8}$$

where M_0 is the mass per unit length of the band, δ is a Dirac function, and θ is a Heaviside step function.

The analysis continues by matching solutions to the right and to the left of the δ function, and then piecing them together: For $x < 0$, Eq. B5 is

$$\omega F = F'' - q^2 F - \frac{M_0}{2} F'.$$

The solution that decays at $-\infty$ is

$$F_< = c e^{\alpha x},$$

where

$$\alpha = \frac{M_0/2 + \sqrt{M_0^2/4 + 4(\omega + q^2)}}{2}.$$

By symmetry, the solution at $+\infty$ is

$$F_> = c e^{-\alpha x}.$$

The eigenvalue condition follows from integrating Eq. B5 across the delta function, yielding the jump condition

$$F_>' - F_<' = \int \rho' G' - 2 \int F \rho_0 - \int c_0'' F$$

$$= (-F(0) - q^2 G(0)) M_0. \tag{B9}$$

The jump condition B9 requires knowing $G(0)$. This is obtained by solving Eq. B6. For $x < 0$,

$$G_< = -\frac{c e^{\alpha x}}{\alpha^2 - q^2} + B e^{qx}.$$

For $x > 0$,

$$G_< = -\frac{c e^{-\alpha x}}{\alpha^2 - q^2} + D e^{-qx}.$$

Continuity of G implies that $B = D$. Continuity of G' implies that

$$\frac{-c\alpha}{\alpha^2 - q^2} + qB = \frac{c\alpha}{\alpha^2 - q^2} - Bq.$$

or

$$B = \frac{c\alpha}{q} \frac{1}{\alpha^2 - q^2},$$

so that

$$G(0) = -\frac{c}{\alpha^2 - q^2} + \frac{c\alpha}{q} \frac{1}{\alpha^2 - q^2} = \frac{c}{q} \frac{1}{\alpha + q}$$

The jump condition B9 then gives

$$-2\alpha = -M_0 - q^2 G(0)/F(0) = -M_0 - \frac{M_0 q}{\alpha + q} \tag{B10}$$

Equation B11 determines $\omega(q)$. Figure 8 plots the growth rate as a function of q (both of which are rescaled in units of M_0).

APPENDIX C: CLUMPING IN LIQUID MEDIUM

A conceptually simpler version of the experiments is to start with an initially uniform distribution of bacteria of density ρ_0 dispersed in a liquid medium, with sufficient succinate that depletion is not an issue. This appendix provides estimates for the number of bacteria per aggregate, and the number of aggregates formed in this situation.

First we proceed with linear analysis. Linearizing the Keller-Segal Eqs. 1 and 2 about the constant state by writing $\rho = \rho_0 + \epsilon e^{\omega t + iqx}$ and $c = \delta e^{\omega t + iqx}$ implies the equations

$$\epsilon\omega = -D_b q^2 \epsilon + k\rho_0 q^2 \delta \tag{C1}$$

$$\delta\omega = -D_c q^2 \delta + \alpha\epsilon. \tag{C2}$$

In the limit of fast diffusion, the growth rate is

$$\omega = \frac{\rho_0 k\alpha}{D_c} - D_b q^2.$$

All modes with wavenumber smaller than the critical wavenumber

$$q* = \sqrt{\frac{\rho_0 k\alpha}{D_c D_c}}$$

will grow. The fastest growing mode occurs with $q = 0$ (i.e., has a wavelength on the order of the box size).

Without taking the limit of fast diffusion, the growth rate (expanded at small q) is

$$\omega = \sqrt{\alpha k\rho_0} q - \frac{D_c + D_b}{2} q^2.$$

The fastest growing mode in this limit has wavelength $\lambda*$:

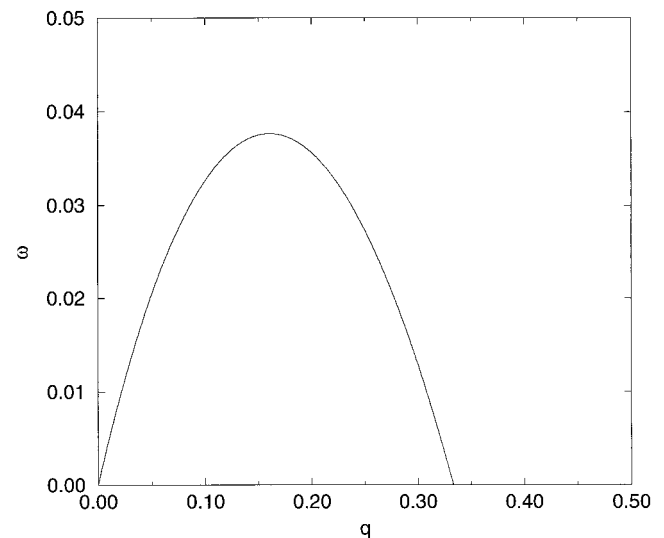$$\lambda* = \frac{2\pi(D_c + D_b)}{\sqrt{\alpha k\rho_0}}.$$

FIGURE 8 Growth rate as a function of q, as determined by Eq. B10. The most unstable mode occurs at $q = 0.15$.

From linear analysis alone, we would expect the bacteria to clump into sections of dimension λ^*, so that the mass of the individual clumps is on the order of $\rho_0(\lambda^*)^3$.

Moreover, if the size of the box containing the bacteria is L, the number of such clumps is

$$N_{\text{clumps}} = \left(\frac{L}{\lambda^*}\right)^3 = \frac{L^3}{8\pi^3}\frac{(\alpha k\rho_0)^{3/2}}{(D_c + D_b)^3}. \qquad \text{(C3)}$$

The most important feature of this result is that linear analysis predicts that the number of clumps scales like $\rho_0^{3/2}$, so that a 100-fold increase in the initial density implies a 1000-fold increase in the number of clumps. This result seemingly contradicts the experimental data reported in the text, which indicate that the number of clumps $N_{\text{clumps}} \approx \rho_0$.

The experiments reported in the text occurred in a quasi-two-dimensional geometry, in which a petri dish with a diameter of a few centimeters was filled with ~5 mm of liquid. The final aggregates had a size on the order of 1 mm, only a few times smaller than the thickness of the layer. Using the numbers for D_b, D_c, k, and α discussed in the text for liquid medium, the critical wavelength $\lambda^* \approx 10^{-1} + 10^{-2}$ cm, depending on the density. There seems to be a discrepancy between this prediction and the numbers measured in the experiments.

A possible reason for this discrepancy is a subtlety in the nonlinear collapse mechanism. To illustrate this, consider the number of clusters created from a hypothetical two-dimensional collapse. According to linear analysis, the number of clumps is

$$N_{\text{clumps}}^{\text{linear,2D}} = \left(\frac{L}{\lambda^*}\right)^2 = \frac{L^2}{4\pi^2}\frac{\alpha k\rho_0}{(D_c + D_b)^2}.$$

On the other hand, as discussed in the text, aggregate formation in two dimensions requires a critical number $D_b D_c/(k\alpha)$ of bacteria. This nonlinear result would predict that the number of clumps

$$N_{\text{clumps}}^{\text{nonlinear,2D}} = \frac{\rho_0 L^2 k\alpha}{D_b D_c}.$$

In two dimensions, both the linear and the nonlinear estimates for the number of clumps have the same scaling with the density ρ_0; the only difference is in the scaling with D_b and D_c. This difference arises from the fact that the finite range of attractant diffusion affects the linear instability, but not the nonlinear threshold for collapse.

In three dimensions, even the scaling of N_{clump} with ρ_0 is affected. The fact that experiments demonstrate $N_{\text{clumps}} \approx \rho_0$ indicates that two-dimensional structures must be determining the number of aggregates in the three-dimensional experiments.

Indeed, experiments in liquid medium indicate that two-dimensional structures (cylinders) always form first, and then destabilize into spherical aggregates. Such dynamics suggest that the number of clumps should be

$$N_{\text{clumps}}^{\text{nonlinear,3D}} = N_{\text{clumps}}^{\text{nonlinear,2D}}\lambda,$$

where λ is the instability wavelength of the cylinder. The calculation of the instability wavelength is beyond the scope of this paper (and will be presented elsewhere). However, note that the nonlinear mechanism implies that the number of bacteria per unit length in each cylinder is $D_c D_b/(k\alpha)$, which is independent of ρ_0! Hence λ will be independent of ρ_0 and $N_{\text{clumps}}^{\text{3D}} \approx \rho_0$.

REFERENCES

Adler, J. 1966. Chemotaxis in bacteria. *Science.* 153:708–716.

Adler, J. 1969. Chemoreceptors in bacteria. *Science.* 166:1588–1597.

Adler, J., and B. Templeton. 1967. The effect of environmental conditions on the motility of *Escherichia coli. J. Gen. Microbiol.* 46:175–184.

Amsler, C. D., M. Cho, and P. Matsumura. 1993. Multiple factors underlying the maximum motility of *Escherichia coli* as cultures enter post-exponential growth. *J. Bacteriol.* 175:6238–6244.

Anderson, K. B., and J. von Meyenburg. 1980. Are growth rates of *Escherichia coli* in batch cultures limited by respiration? *J. Bacteriol.* 144:114–123.

Ben-Jacob, E., I. Cohen, O. Shochet, I. Aranson, H. Levine, and L. Tsimring. 1995. Complex bacterial patterns. *Nature.* 373:566–567.

Berg, H. C. 1988. A physicist looks at bacterial chemotaxis. *Cold Spring Harb. Symp. Quant. Biol.* 53:1–9.

Berg, H. C., and D. A. Brown. 1972. Chemotaxis in *Escherichia coli* analysed by three dimensional tracking. *Nature.* 239:500–504.

Berg, H. C., and L. Turner. 1990. Chemotaxis of bacteria in glass capillary arrays. *Biophys. J.* 58:919–930.

Blair, D. F., and H. C. Berg. 1988. Restoration of torque in defective flageller motors. *Science.* 242:1678–1681.

Block, S., and H. C. Berg. 1984. Successive incorporation of force-generating units in the bacterial rotary motor. *Nature.* 309:470–472.

Bonner, J. 1967. The Cellular Slime Molds. Princeton University Press, Princeton, NJ.

Bruno, W. 1992. *CNLS Newsletter.* 82:1–10.

Budrene, E., and H. Berg. 1991. Complex patterns formed by motile cells of *Escherichia coli. Nature.* 349:630–633.

Budrene, E. O., and H. Berg. 1995. Dynamics of formation of symmetrical patterns by chemotactic bacteria. *Nature.* 376:49–53.

Burgers, J. M. 1948. A mathematical model illustrating the theory of turbulence. *Adv. Appl. Mech.* 1:171–199.

Childress, S. 1984. Chemotactic collapse in two dimensions. *Lect. Notes Biomath.* 55:61–68.

Childress, S., and J. Percus. 1981. Nonlinear aspects of chemotaxis. *Math. Biosci.* 56:217–237.

Dahlquist, F. W., P. Lovely, and K. E. Koshland. 1972. Qualitative analysis of bacterial migration in chemotaxis. *Nature New Biol.* 236:120–123.

Herrero, M. A., and J. J. L. Velazquez. 1996. Singularity patterns in a chemotaxis model. *Math. Ann.* 308:583–622.

Hofer, T., and P. K. Maini. 1997. Streaming instability of slime mold amoebae: an analytical model. *Phys. Rev. E.* 56:2074–2080.

Hofer, T., J. A. Sherratt, and P. Maini. 1995. Cellular pattern formation during dictyostelium aggregation. *Proc. R. Soc. Lond.* 259:425–444.

Keller, E., and G. Odell. 1975. Necessary and sufficient conditions for chemotactic bands. *Math. Biosci.* 270:309–317.

Keller, E., and L. Segel. 1970. Initiation of slime mold aggregation viewed as an instability. *J. Theor. Biol.* 26:399–415.

Kessler, D. A., and H. Levine. 1993. Pattern formation in dictyostelium via the dynamics of cooperative biological entities. *Phys. Rev. E.* 48:4801–4804.

Khan, S., and R. M. Macnab. 1980. Proton chemical potential, proton electrical potential, and bacterial motility. *J. Mol. Biol.* 138:599–614.

Lee, K., E. Cox, and R. E. Goldstein. 1996. *Phys. Rev. Lett.* 76:1174–1177.

Murray, J. 1989. Mathematical Biology. Springer Verlag, Berlin.

Nanjudiah, V. 1973. Chemotaxis, signal relaying and aggregation morphology. *J. Theor. Biol.* 42:63–105.

Oster, G. and J. D. Murray. 1989. Pattern formation models and developmental constraints. *J. Exp. Zool.* 251:186–202.

Pfeffer, W. 1884. *Untersuch. Bot. Inst. Tubingen.* 1:363.

Raschle, M., and C. Ziti. 1995. Finite time blow-up in some models of chemotaxis. *J. Math. Biol.* 33:388–414.

Reitzer, L. J. 1996. Ammonia assimilation and the biosynthesis of glutamine, glutamate, aspartate, asparagine, L-alanine and D-alanine. *In*

Escherichia coli and *Salmonella*, F. C. Neidardt, editor. ASM Press, Washington, DC.

Schnitzer, M. J. 1993. Theory of continuum random walks and application to chemotaxis. *Phys. Rev. E.* 48:2553–2568.

Schnitzer, M. J., S. Block, H. Berg, and E. Purcell. 1990. *Symp. Soc. Gen. Microbiol.* 46:15.

Segall, J. E., S. Block, and H. C. Berg. 1986. Temporal comparisons in bacterial chemotaxis. *Proc. Natl. Acad. Sci. USA.* 83:8987–8991.

Stock, J. B., and M. G. Surette. 1996. Chemotaxis. *In Escherichia coli* and *Salmonella*, F. C. Neidardt, editor. ASM Press, Washington, DC. 1103–1129.

Tsimring, L., H. Levine, I. Aranson, E. B. Jacob, I. Cohen, O. Shochet, and W. Reynolds. 1995. Aggregation patterns in stressed bacteria. *Phys. Rev. Lett.* 75:1859–1862.

Turing, A. 1952. The chemical basis of morphogenesis. *Proc. R. Soc. Lond.* 237:37–72.

Tyson, R. 1996. Pattern formation by *E. coli*—mathematical and numerical investigation of a biological phenomenon. Ph.D. thesis. University of Washington, Seattle.

Vasiev, B. N., P. Hogeweg, and A. V. Panfilov. 1994. Simulation of dictyostelium discoideum aggregation via reaction diffusion model. *Phys. Rev. Lett.* 73:3173–3176.

Wolfe, A. J. and H. Berg. 1989. Migration of bacteria in semi-solid agar. *Proc. Natl. Acad. Sci. USA.* 86:6973–6977.

Woodward, D. E., R. Tyson, M. Myerscough, J. D. Murray, E. Budrene, and H. Berg. 1995. Spatio-temporal patterns generated by salmonella. *Biophys. J.* 68:2181–2189.